Theoretical and experimental investigations of nano-Schottky contacts

Moh'd Rezeq,[1,2,a)] Khouloud Eledlebi,[1] Mohammed Ismail,[1] Ripon Kumar Dey,[2] and Bo Cui[2]
[1]*Department of Electrical and Computer Engineering, and KSRC, Khalifa University of Science Technology and Research, POB 127788 Abu Dhabi, United Arab Emirates*
[2]*Department of Electrical and Computer Engineering, University of Waterloo, Waterloo, Ontario N2L 3G1, Canada*

(Received 19 May 2016; accepted 7 July 2016; published online 22 July 2016)

Formation of metal-semiconductor (M-S) contacts at sub-20 nanometer range is a key requirement for down-scaling of semiconductor devices. However, electrical measurements of M-S contacts at this scale have exhibited dramatic change in the current-voltage (I-V) characteristics compared to that of conventional (or planar) Schottky contacts. This change is actually attributed to the limited metal contact region where the transferred charge from the semiconductor into the metal is confined to a small surface area, which in turn results in an enhanced electric field at the nano-M-S interface. We here present detailed theoretical models to analyze the nano-M-S junctions at 10 nm contact range and then implement this analysis on the experimental data we conducted under these conditions. Both theoretical and experimental results demonstrate a significant effect of the contact size on the electronic structure of the M-S junctions and thus on the I-V characteristics. This effect is rather prominent when the size of the metal contact is substantially smaller than the width of conventional depletion region of the relevant planar M-S contacts. *Published by AIP Publishing.*
[http://dx.doi.org/10.1063/1.4959090]

I. INTRODUCTION

Nano metal-semiconductors (M-S) contacts have a wide range of prospective applications in several aspects of nano-technology, particularly in nano-electronics, due to the current trend in down-scaling of semiconductor devices. Therefore, understanding the electronic characteristic of such nano interfaces is crucial. Some experimental and theoretical analyses have been made to investigate the nano M-S contacts.[1–16] The analyses have addressed the effect of the nano contact size on the depletion width and on other interface parameters. It was reported that I-V characteristics showed an enhanced current in the reverse bias, which can be attributed to the enhancement of the electric field at the nano M-S interface due to the confined electric charge on a very small metal surface area.[15,16] This enhancement of the tunneling current can lead to a reversed rectification diode behavior if the contact size is very small, sub-10 nm range, as will be demonstrated here both theoretically and experimentally.

To analyze the nano M-S interface, the main parameter to be determined is the depletion width in the semiconductor side of the M-S interface. This would help to figure out the other parameters like the interface potential and electric field. These parameters will, in turn, be used to calculate the electric current at various applied biases. Here, we present theoretical analyses of the nano-M-S interface by calculating the depletion region for various nano M-S contacts. We have used two approaches to calculate the depletion region. The first approach is based on the conventional method of solving Poisson's equation after defining the boundary conditions at both sides of the depletion region, as also considered in a previous work.[15,16] We have found out that although this approach predicts an enhanced tunneling current in the reverse bias, it cannot fit the I-V data for extremely small M-S contacts. Therefore, we proposed another approach to analyze nano Schottky contacts based only on the equilibrium state at the nano-M-S interface and the alignment of the Fermi levels in the semiconductor and the metal sides, without pinning the potential at the barrier height value at the interface.[17] We show here that the latter approach provides better data fit particularly when the contact size is much smaller than the conventional depletion region. For instance, for low doped n-type substrates (dopant concentration $N_d \cong 1 \times 10^{16}\,cm^{-3}$), the new approach gives a reasonable data fit when the radius of the contact is around 10 nm.

II. THEORETICAL MODELS AND ANALYSIS OF NANO-SCHOTTKY CONTACTS

For feasible analysis of M-S Schottky contacts at nano-scale, we build a model of a spherical geometry to utilize the spherical symmetry of the system. We visualize the metal contact as a nano metal sphere embedded in a semiconductor bulk. Since the nano M-S contacts take place on the surface of the semiconductor substrate, this can be visualized as if the model of the nano- metal sphere in the center semiconductor bulk is cut into two identical halves. Each half represents a hemispherical nano metal particle embedded on the surface of a substrate, as depicted in Fig. 1.

A. Nano Schottky contacts analysis: Conventional approach (approach 1)

In the conventional approach of analysis of such nano M-S contacts, the potential at the interface is considered to be pinned at the barrier height divided by the electron charge

a)Author to whom correspondence should be addressed. Electronic mail: mohd.rezeq@kustar.ac.ae

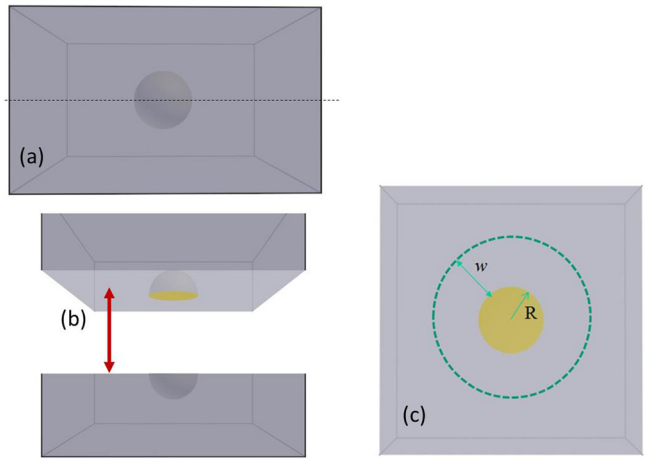

FIG. 1. (a) and (b) A model of a nano metal sphere in the center of a semiconductor bulk and then it is cut along the horizontal plane (dashed line) passing through the center of the nano particle. (c) Top view of a 2D model of a hemispherical nano particle embedded in the surface of a semiconductor substrate after cutting the model into two identical parts.

(i.e. $V=-\phi_B$), which drops gradually to reach the value $(-\phi_s)$ at the end of the depletion region, as schematically shown in Fig. 2. We use these boundary conditions in Poisson's equation to solve for the depletion region (W_n). Poisson's equation in spherical coordinates is given by

$$\nabla V^2 = -\frac{\rho}{\mathcal{E}_S} = \frac{1}{r^2}\frac{\partial}{\partial r}\left(r^2\frac{\partial V}{\partial r}\right)+\frac{1}{r^2\sin\theta}\frac{\partial}{\partial\theta}\left(\sin\theta\frac{\partial V}{\partial\theta}\right)+\frac{1}{r^2\sin^2\theta}\frac{\partial^2 V}{\partial\varphi^2}, \quad (1)$$

where ρ is the volume charge density, $\rho = eN_d$ (absolute value).

Since the model is symmetric in the spherical coordinate system, the potential and hence the electric field are independent of the angles θ or φ. Consequently, Equation (1) can be reduced to

$$\nabla V^2 = \frac{1}{r^2}\frac{\partial}{\partial r}\left(r^2\frac{\partial V}{\partial r}\right) = -\frac{\rho}{\mathcal{E}_S}. \quad (2)$$

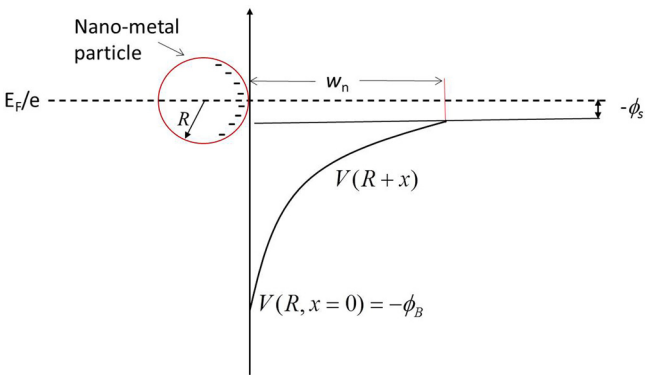

FIG. 2. A schematic of the potential profile inside the semiconductor depletion region due to the nano M-S contact.

The derivation of the potential at the interface is detailed in Appendix A. The potential profile function at the nano M-S interface inside semiconductor region is given as

$$V(R+x)=\frac{\rho}{3\mathcal{E}_S}\left\{\frac{3(R+W_n)^2}{2}-\frac{(R+x)^2}{2}-\frac{(R+W_n)^3}{(R+x)}\right\}-\phi_s. \quad (3)$$

To find W_n, we apply the boundary conditions on Equation (3), where at the M-S interface, i.e., $r=R$ (or $x=0$), $V(R)=-\phi_B$ (in the absence of the external applied voltage), and at the end of the depletion region ($r=R+W_n$), the potential $V(R+W_n)=-\phi_s$. The calculations of W_n from Equation (3) for a wide range of metal spheres radii are presented in Fig. 3. The results show that W_n increases smoothly from a small value until it reaches the conventional value at a large radius. However, when an external voltage is applied on the metal, the new boundary potential at the M-S interface becomes $V(R)=-\phi_B+V_a$.

B. Nano Schottky contacts analysis: Modified approach (approach 2)

In the case of extremely small metal contacts, the confined charge transferred to the metal at the equilibrium state may results in an interface potential higher than the barrier height. In this regime, the potential at the interface is presumed to depend on the surface charge density accumulated at the metal side and hence on the radius of the nano metal particle. Therefore, finding the depletion width and other interface parameters is not straightforward. Instead, we have proposed a qualitative method based on the evolution of the potential profile in the semiconductor as the contact size is decreasing from the planar contact to sub-10 nm range. When the metal contact has a limited radius, the charge density will be enhanced, which results in an enhanced surface potential that drops almost exponentially with the decrease of the metal sphere radius. The evolution of the potential

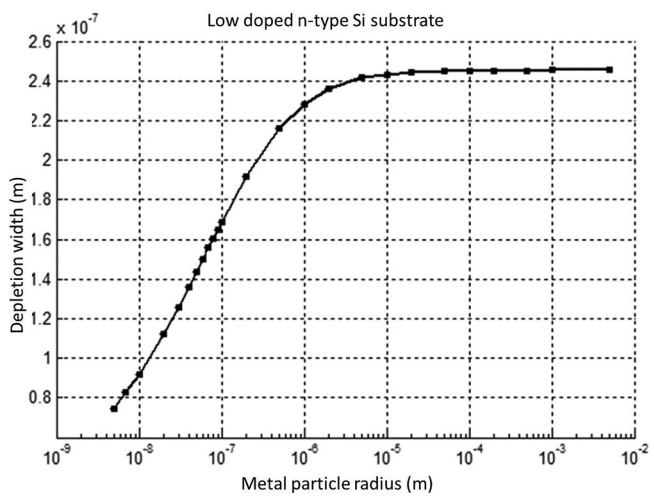

FIG. 3. The depletion width W_n as the metal sphere radius increases from 3 nm to 50 μm for a low doped n-type Si substrate ($N_d = 1\times10^{16}$ cm^{-3}). The horizontal scale is logarithmic.

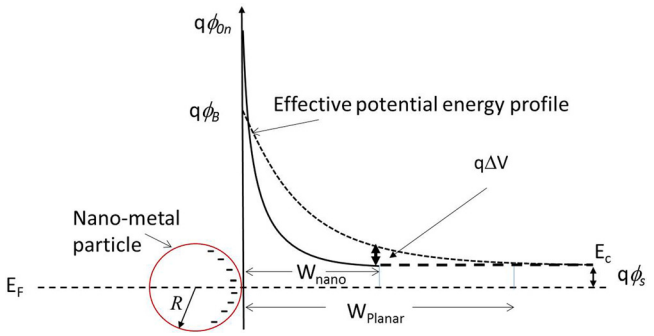

FIG. 4. The effect of the high surface charge density on the metal nanoparticle due to the reduction in the depletion width from the planar value, which results in an enhancement of the potential energy at the interface from the planar value $q\phi_B$ to a value of $q\phi_{0n}$.[14]

energy diagram is illustrated schematically in Fig. 4, where $q\phi_{0n}$ denotes the new surface potential energy.

The new nano-depletion region (W_n) is associated with a drop in the potential energy at this point equals to qΔV (q here is the electron's charge). To calculate W_n, we recall the nature of the potential profile in the semiconductor bulk which is a result of the superposition of the potential from the positive region in the bulk and the negative potential from the metal. Assuming that at the equilibrium state the Fermi levels on both sides of the M-S contact are aligned up, we can visualize that the drop of the potential from the Fermi level of the semiconductor (before contact) to the metal level at the interface (after contact) is a result of the increase of the positive potential in the semiconductor due to the transfer of the negative charge to the metal. This drop is assumed to be equal to the difference between the Fermi levels in both sides (V_{bi}) before the physical contact. Based on this assumption, the positive potential profiles in the semiconductor, as the contact is reduced from planar to nano scale range, are represented in Fig. 5.

Figure 5 illustrates the change of the negative net electric potential from $V_p(x)$ of planar M–S contacts (dashed blue line) to the new potential $V_n(R+x)$ for nano M–S contacts (green line), where $V_p(x)$ can be derived easily by solving Poisson's equation with the fixed boundary conditions and is given by

$$V(x) = \frac{\rho}{\varepsilon_s}\left(\frac{W_P{}^2}{2} - W_P x + \frac{x^2}{2}\right) - \phi_S \quad \text{when } 0 \le x \le W_P. \tag{4}$$

$V_P^+(x)$ shows the positive potential profile in the semiconductor for the planar M-S contact. This positive potential profile $V_P^+(x)$ can be readily found from Gauss's Law of the electric field flux, as given by

$$V_P^+(x) = V_{bi} - \frac{\rho_v x^2}{2\varepsilon_s}. \tag{5}$$

The positive potential profile in the semiconductor for the nano M-S contact ($V_n^+(x)$) is also given in Equation (6) and detailed in Appendix B (and depicted in Fig. 10)

$$V_n^+(R+x) = V_{bi} - \frac{\rho}{3\varepsilon_s}\left[\frac{(R+W_n)^2}{2} + \frac{R^3}{R+W_n} - \frac{3R^2}{2}\right]. \tag{6}$$

From the schematics in Fig. 5, we can assume that the drop of the net potential in the bulk (ΔV) is proportional to the enhancement of the positive potential in the semiconductor bulk ($\Delta V'$). Thus

$$\Delta V' = B\Delta V, \tag{7}$$

where B is a real constant value that can be determined by fitting the experimental data of the I-V measurements. From Fig. 5, ΔV is found to be

$$\begin{aligned}\Delta V &= V_P(x) + \phi_S = -(V_{bi} + \phi_S) - \frac{\rho x^2}{2\varepsilon_S} + \varepsilon_S \rho W_p x + \phi_S \\ &= -V_{bi} - \frac{\rho x^2}{2\varepsilon_S} + \varepsilon_S \rho W_p x.\end{aligned} \tag{8}$$

To find the value of the new depletion region (W_n) when $V_n(x)$ reaches $-\phi_S$, at $x = W_n$, the following equation should apply:

$$\Delta V' = V_n^+(x) - V_P^+(x) = \mathrm{B}\Delta V. \tag{9}$$

We solve this equation numerically using a Matlab program to find the modified depletion region (W_n) for a given radius (R) at a given B. The B factor is actually dependent on the tip radius and can be extracted by fitting the experimental data. As an example, for nano-tips with a radius around 10 nm in contact with a low-doped substrate, we found that the best value for B is 0.55, as we will show later in this paper.

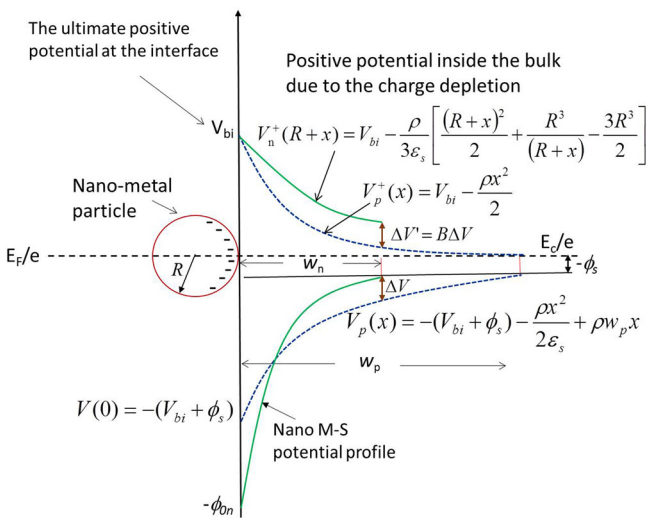

FIG. 5. Schematics of the potential profiles for the conventional M-S contacts and the modified model of nano Schottky contacts.

III. EXPERIMENTAL PROCEDURE AND MEASUREMENTS

Nano M-S contacts were investigated using conductive-mode Atomic Force Microscope (AFM). To ensure better conductivity through the AFM probe, the tip was coated with 5–20 nm of gold by electron beam evaporation technique, after being covered with 5 nm of Cr to enhance the

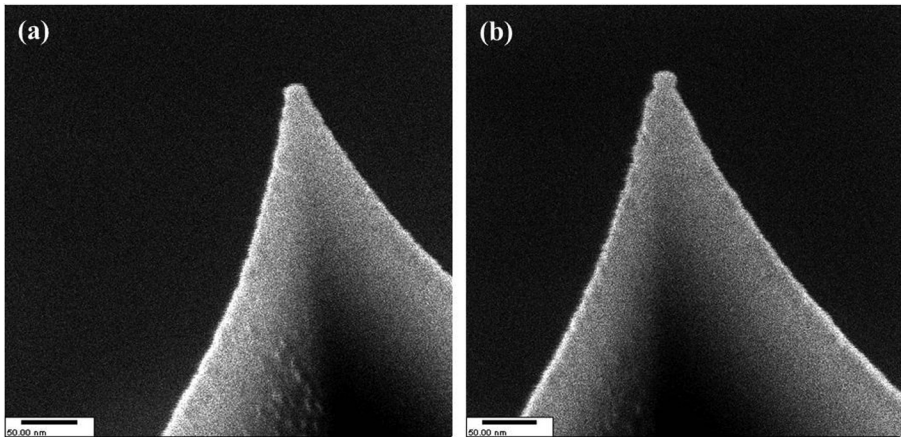

FIG. 6. (a) and (b) Scanning Helium Ion Microscope images of AFM tips coated with gold. The estimated apex radius of each of these tips is around 10 nm.

conductivity. Tips with a well-defined conical shape and a radius within the range of 8–10 nm had been chosen for the experiments. Helium Ion Microscope (HIM) images of such tips are shown in Fig. 6. These Au coated tips were estimated from HIM images to have a radius of apex around 10 nm, as shown in Figs. 6(a) and 6(b).[17]

The I-V measurements were performed on two n-type Si materials: low doped (5–10 Ω cm) and highly doped (0.02–0.04 Ω cm). The Si samples have (100) crystal orientation and their thickness is 375 ± 20 μm. Carbon black material was used on the back side of the Si to ensure good contact with the sample metal stage. In order to improve the physical contact between Au coated AFM tips and Si surface, the native oxide on the Si surface was removed by diluted HF solution before characterizations. Here, a typical deflection negative voltage (−2 V) from the setpoint is applied to maintain a constant positive cantilever pressure on the sample.

We would like to indicate here that other methods can be used to form nano-Schottky contacts by incorporating the metallization process in high resolution lithography techniques, for example, enhanced sub-wavelength photolithography, and ion and electron beam lithography.

We have two sets of measurements prepared in different sessions from different samples. However, we can classify them into two groups based on their contact resistances, set 1 and set 2, where set 2 showed greater contact resistance than set 1. In general, the I-V curves have showed an enhanced tunneling current in the reverse bias and a small current at the forward bias for low n-doped substrates, whereas for highly n–doped substrates, I-V curves exhibit a conventional Schottky diode behavior.[18–21]

IV. EXPERIMENTAL RESULTS AND THEORETICAL DATA

Before discussing the experimental results, it is worth introducing the method we used to calculate the electric current in forward and reveres biases. When the AFM nanoprobe is making a physical contact with the substrate under an applied voltage, the electric current can take two paths, one over the surface due to the surface conductance and the other current is going through the bulk, which encounters the diode resistance and the contact resistance (R_s), in series, as illustrated in the schematic in Fig. 7. Therefore, the total current is the summation of the nano-diode current (I_d) and the surface current (I_L)

$$I_{tot} = I_d + I_L, \tag{10}$$

where I_L simply equals V_{app}/R_L (R_L is the surface resistance). For the calculation of I_d, we are considering the dominant nano- junction current, namely, the thermionic current I_{th} and the tunneling current I_{tun}, which are given in the following established equations:[21,22]

$$I_{th} = AA^*T^2 e^{\left[\frac{-q\phi_b}{kT}\right]}\left[e^{\frac{qV_d}{nkT}} - 1\right], \tag{11}$$

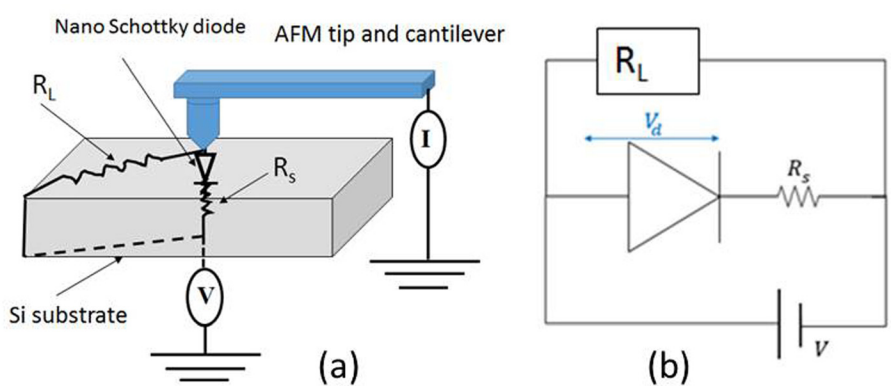

FIG. 7. Schematics showing (a) a nano-tip in contact with a semiconductor substrate and (b) the equivalent circuit representation of the nano-diode, series resistance, and surface resistance. R_L in the schematics and the circuit is the surface resistance and R_s is the contact resistance.

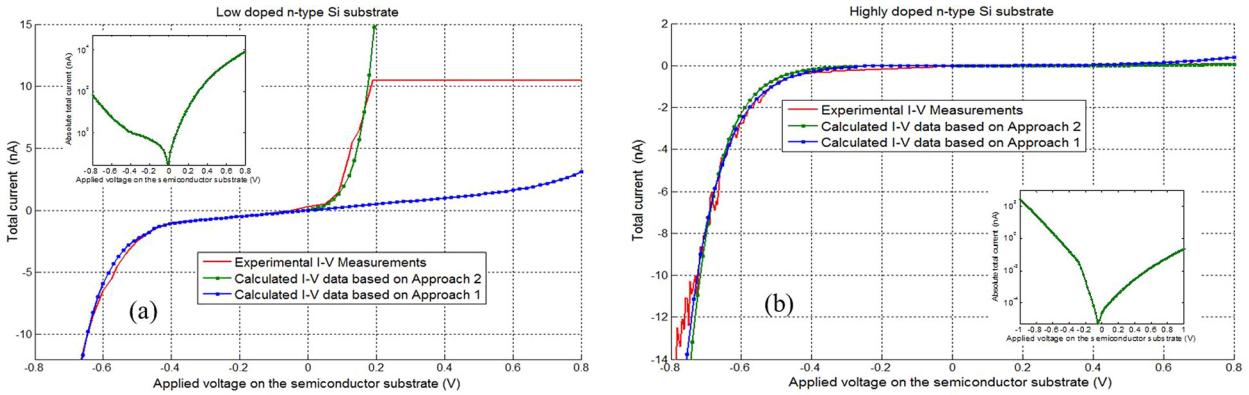

FIG. 8. I-V data for low resistance nano Schottky contact on (a) low n-doped semiconductor substrate ($N_d \cong 1 \times 10^{16}\,cm^{-3}$), the flat horizontal red line is due to the electronics amplifier saturation value. (b) Highly n-doped semiconductor substrate ($N_d \cong 1 \times 10^{18}\,cm^{-3}$). The inserts in (a) and (b) show the I-V data in semi-log plots of the best data fit curves.

$$I_{tun} = A\,\frac{q^2E_{max}^2}{8\pi h(\phi_b)}\,e^{\left[-\frac{8\pi}{3hqE_{max}}\sqrt{2m^*(q\phi_b)^3}\right]}, \tag{12}$$

where A is the area of the nano M-S contact, A^* is Richardson constant ($A^* = 112\,\frac{A}{cm^2K^2}$), ϕ_b is the effective potential at the barrier height, V_a is the bias voltage, k is Boltzmann constant ($k = 1.3806488 \times 10^{-23}\,J\,K^{-1}$), m^* is the effective electron mass in the semiconductor, n is the concentration of electrons, E_{max} is the maximum electric field at the interface, h is Planck constant and equals 6.62617 $\times 10^{-34}$ J s, and T is the room temperature (T = 300 K).

A. Results of set 1 measurements

The I-V measurements were performed on a low n–doped Si substrate. When the tip was making a physical contact with the substrate, the voltage was swept between −0.8 V and 0.8 V. The experimental data is represented in Fig. 8(a) (denoted by red solid curve). The data clearly show that the tunneling current in the reverse bias is enhanced dramatically from a very small value at 0.1 V to around 12 nA at 0.2 V. Whereas in the forward bias, the current initially increases slowly before the turning point at −0.40 V. Fig. 8(a) clearly shows a reversed rectification Schottky diode behavior for low n–doped Si substrates.

The same measurements were performed on a highly n-doped Si substrate, and the data are presented in Fig. 8(b). We can readily notice from the experimental data that the I-V behavior (red solid curve) is similar to the conventional nano-Schottky diode I-V characteristics, where the current in the reverse bias is almost negligible and the current in the forward bias is dominant.

To verify the validity of both approaches, we tried to fit the experimental data, especially in the reverse bias where the nano-contact size has a significant effect on the tunneling current. However, we started by checking the experimental I-V data at the forward bias to extract some crucial parameters like the contact resistance and contact area, and then we used these parameters in our theoretical model to calculate the current in the reverse bias. Since the electric field in the forward bias is too small for the tunneling current to occur, we expect the thermionic current to be dominant. Here, we estimated the contact resistance by assuming that the diode resistance decreases as the applied voltage increases. Therefore, at a relatively high forward bias, above 0.6 V, the current slope is substantially affected by the contact resistance. For reasonable approximation, we calculated the slope of the last portion of the curve, $R_S = \frac{\Delta V}{\Delta I}$, after drawing a fitting line to minimize the noise effect. R_S is estimated from Fig. 8(b) to be around 15 MΩ. To estimate the area of contact, we choose a point on the I-V curve in forward bias, and then we calculate the effective applied voltage on the diode as $V_d = V - V_R$, where $V_R = I_dR_s$. Later, we used this value V_d in the thermionic current equation, Equation (11), to calculate the contact area (A) that gives the same current, which was found to be around 15 nm^2. In fact, the contact area depends on the nanotip radius, and practically, it has to be less than the circular surface area (A_c) of the hemisphere of the tip apex, i.e., $A_c = \pi R^2$.

Referring to Equation (10), we estimated the value R_L from the linear part of the red curve in Fig. 8(a). This is done since the dominant current at small voltages is the leakage current. We selected a small range (V, I_{tot}) and found R_L from $\frac{\Delta V}{\Delta I_{tot}}$ to be around 400–500 MΩ. Later, we used these parameters (mainly R_S, A, R_L) to calculate the tunneling current based on the theoretical model using both approaches, the conventional and the modified approaches. We used the value of R_S to calculate the effective potential drop on the diode by considering the difference between the experimental applied voltage (V), after deducting the leakage current value, and the voltage drop on the contact resistance (V_R), as follows:

$$V_d = V - I_dR_S. \tag{13}$$

By using the previous contact parameters in approach 1 (the conventional approach), the I-V data are presented in Fig. 8(a) (blue solid curve). We also used the same parameters in approach 2 (the modified approach) and selected B factor to be 0.55 to obtain the best fitting curve, as shown in Fig. 8(a) (green solid curve). Note that the data based on

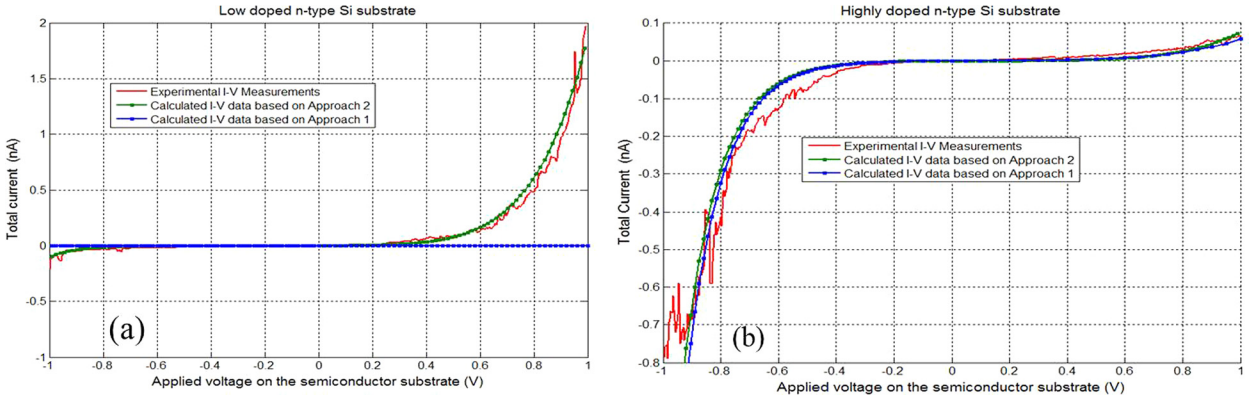

FIG. 9. I-V data for high resistance nano Schottky contact on (a) low n-doped semiconductor substrate and (b) highly n-doped semiconductor substrate.

approach 2 give better fitting to the experimental measurements than the conventional approach. For more clarity, the insert in Fig. 8(a) shows a semi-log plot of the best fit of I-V data from approach 2.

The previous procedures were repeated to fit the experimental data for highly n–doped Si substrate. The experimental data exhibit a very small surface leakage current, which indicates a high surface resistance. We, therefore, considered the surface conductance to be negligible. The value of R_S was also found to be around 30 MΩ, and the contact area remained the same as found from the previous fitting, while the best value of (n) was kept at unity, n = 1. By implementing both approaches (approach 1 and 2) on highly n-doped Si substrate, it was noticed that there is no such difference in their I-V behavior at the forward bias. This is because in both models, the thermionic current is dominant at the forward bias and the tunneling current is very small in the reverse bias. The theoretical and experimental results are depicted in Fig. 8(b). The insert in Fig. 8(b) shows the semi-log plot of the I-V data fit from approach 2.

B. Results of the set 2 measurements

For this group of I-V measurements, the current value is less than that obtained in the previous set, which indicates a higher contact resistance. This may be due to some factors like surface contaminations. The I-V measurements were conducted for low n-doped and highly n-doped Si substrates, over a voltage range from −1.0 to 1.0 V. The experimental data for low n-doped Si substrate is presented in Fig. 9(a) (denoted by red solid curve). The data clearly showed an enhancement in the tunneling current in the reverse bias and a very small current in the forward bias, hence a reversed rectification behavior compared to conventional Schottky contacts. The same measurements were performed on a highly n–doped Si substrate, and the data are presented in Fig. 9(b). We can easily notice that the experimental I-V data (red solid curve) is similar to the conventional I-V characteristics, where the current in the reverse bias is almost negligible and the current in the forward bias is dominant.

We used the same approach to fit that data for this set of measurements. We found the estimated series resistance value to be around 590 MΩ. The contact area is the same as in the previous group. The experimental data indicates a negligible contribution of the surface leakage current. We also found out the best data fit is achieved when the value of the ideality factor (n) is 1.0. The I-V data from the conventional approach (blue solid curve) showed a quite small reverse current, while the data are best fit using the modified approach when we select a B factor to be 0.55 (green solid curve). When fitting the experimental data for the highly n-doped Si substrate, the experimental data also indicates a negligible surface contribution. The value of R_S was found to be 750 MΩ, with the same contact area and n = 1.

V. CONCLUSION

We have studied experimentally the nano-Schottky contacts for two different doped n-type Si substrates, low doped ($\sim 1 \times 10^{16}$ cm^{-3}) and highly doped ($\sim 1 \times 10^{18}$ cm^{-3}). The results showed obviously an enhanced tunneling current in the reversed bias for nano M-S contacts with low n-doped Si, whereas a conventional diode behavior has been observed for highly n-doped Si. This indicates a significant effect of the contact size on the electronic structure of M-S junctions when the nano contacts radii are much smaller than the conventional M-S interface depletion width. We have also used theoretical models to thoroughly investigate the electrical characteristics of nano M-S interfaces and developed a new approach that fit well the experimental data.

ACKNOWLEDGMENTS

This research was supported by ATIC-SRC contract number 2012-VJ-2333.

APPENDIX A: DERIVATION OF THE POTENTIAL PROFILE AT NANO M-S INTERFACE USING THE CONVENTIONAL APPROACH

In this approach, the potential at the interface is considered to be the barrier height divided by the charge (ϕ_B). Inside the bulk (at the end of the depletion region), the potential is ϕ_S. We use these parameters in Poisson's equation to solve for the potential profile in the depletion region. Poisson's equation in spherical coordinates is defined by

$$\nabla V^2 = -\frac{\rho}{\mathcal{E}_S} = \frac{1}{r^2}\frac{\partial}{\partial r}\left(r^2\frac{\partial V}{\partial r}\right) + \frac{1}{r^2\sin\theta}\frac{\partial}{\partial\theta}\left(\sin\theta\frac{\partial V}{\partial\theta}\right) + \frac{1}{r^2\sin^2\theta}\frac{\partial^2 V}{\partial\varphi^2}. \quad \text{(A1)}$$

Since the model is symmetric in the spherical coordinate system, the potential and hence the electric field do not change with the change of θ or φ. Consequently, the equation can be reduced to be dependent on one variable (r)

$$\nabla V^2 = \frac{1}{r^2}\frac{\partial}{\partial r}\left(r^2\frac{\partial V}{\partial r}\right) = -\frac{\rho_v}{\mathcal{E}_S}. \quad \text{(A2)}$$

The first integration gives us the following result for the electric field:

$$r^2\frac{\partial V}{\partial r} = -\frac{\rho}{\mathcal{E}_S}\frac{r^3}{3} + c, \quad \text{(A3)}$$

$$\frac{\partial V}{\partial r} = -\frac{\rho}{\mathcal{E}_S}\frac{r}{3} + \frac{c}{r^2}. \quad \text{(A4)}$$

Since

$$\frac{\partial V}{\partial r} = -E(r) \quad \text{(A5)}$$

then

$$E(r) = \frac{\rho}{\mathcal{E}_S}\frac{r}{3} - \frac{c}{r^2}. \quad \text{(A6)}$$

Assuming the depletion width for the nano M-S contact is W_n, the electric field at $r = R + W_n$ is zero. Then

$$\frac{\rho}{\mathcal{E}_S}\frac{(R+W_n)}{3} - \frac{C}{(R+W_n)^2} = 0, \quad \text{(A7)}$$

$$c = \frac{\rho}{3\mathcal{E}_S}(R+W_n)^3. \quad \text{(A8)}$$

The potential will then be

$$\int_{V(R+x)}^{V(R+W_n)} dv = \int_{R+x}^{R+W_n}\left[-\frac{r\rho}{3\mathcal{E}_S} + \frac{\rho}{3\mathcal{E}_S}\frac{(R+W_n)^3}{r^2}\right]dr, \quad \text{(A9)}$$

$$V(R+W_n) - V(R+x) = \frac{\rho}{3\mathcal{E}_S}\left(\frac{-r^2}{2} - \frac{(R+W_n)^3}{r}\right)\Bigg|_{R+x}^{R+W_n}, \quad \text{(A10)}$$

$$V(R+x) = \frac{\rho}{3\mathcal{E}_S}\left\{\left(\frac{(R+W_n)^2}{2} + \frac{(R+W_n)^3}{(R+W_n)}\right) - \left(\frac{(R+x)^2}{2} + \frac{(R+W_n)^3}{(R+x)}\right)\right\} + V(R+W_n), \quad \text{(A11)}$$

$$V(R+x) = \frac{\rho}{3\mathcal{E}_S}\left\{\frac{3(R+W_n)^2}{2} - \frac{(R+x)^2}{2} - \frac{(R+W_n)^3}{(R+x)}\right\} - \phi_S. \quad \text{(A12)}$$

APPENDIX B: DERIVATION OF THE POSITIVE POTENTIAL PROFILE IN THE SEMICONDUCTOR FOR THE NANO M-S CONTACT ($V_n^+(x)$)

To find the potential profile for the schematic in Fig. 10, we consider the electric flux and Gauss's law as follows:

$$\int \boldsymbol{E}.d\boldsymbol{A} = \frac{Q}{\varepsilon_s} = 4\pi r^2 E = \frac{4\pi\rho}{3\varepsilon_s}(r^3 - R^3). \quad \text{(B1)}$$

This gives

$$E = \frac{\rho}{3\varepsilon_s}\left[r - \frac{R^3}{r^2}\right]. \quad \text{(B2)}$$

Knowing that $E = -\frac{dV}{dr}$, then

$$\int_R^r dV = -\int_R^r E.dr = V(r) - V(R), \quad \text{(B3)}$$

$$V(r) - V(R) = -\frac{\rho}{3\varepsilon_s}\left[\frac{r^2}{2} + \frac{R^3}{r}\right]\Bigg|_R^{R+x} = \frac{-\rho}{3\varepsilon_s}\left[\left(\frac{(R+x)^2}{2} + \frac{R^3}{R+x}\right) - \left(\frac{R^2}{2} + R^2\right)\right] = \frac{-\rho}{3\varepsilon_s}\left[\frac{(R+x)^2}{2} + \frac{R^3}{R+x} - \frac{3R^2}{2}\right], \quad \text{(B4)}$$

$$V(r) = V(R) - \frac{\rho}{3\varepsilon_s}\left[\frac{(R+x)^2}{2} + \frac{R^3}{R+x} - \frac{3R^2}{2}\right]. \quad \text{(B5)}$$

Since $V(R) = V_{bi}$, and $V(r) = V(R+x)$ then Eq. (B5) can be written as

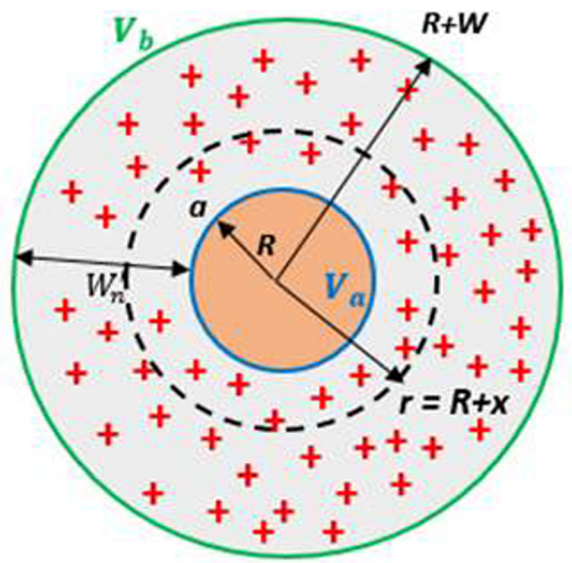

FIG. 10. Schematics showing the depletion region of nano M-S contact as a spherical shell surrounding the nano metal particle.

$$V_n^+(R+x) = V_{bi} - \frac{\rho}{3\varepsilon_s}\left[\frac{(R+x)^2}{2} + \frac{R^3}{R+x} - \frac{3R^2}{2}\right]. \quad \text{(B6)}$$

[1]S.-K. Lee, C.-M. Zetterling, M. Ostling, I. Aberg, M. H. Magnusson, K. Deppert, L.-E. Wernersson, L. Samuelson, and A. Litwin, "Reduction of the Schottky barrier height on silicon carbide using Au nano-particles," Solid-State Electron. **46**, 1433–1440 (2002).

[2]J. Q. Song, T. Ding, J. Li, and Q. Cai, "Scanning tunneling microscope study of nanosized metal-semiconductor contacts between $ErSi_2$ nanoislands and Si(001) substrate," Surf. Sci. **604**, 361–365 (2010).

[3]M. Achermanna, U. Siegnerb, L.-E. Wernerssonc, and U. Kellera, "Nanoscale Schottky contacts: Ultrafast drift-diffusion dynamics studied in the optical near field," Physica E **13**, 819–822 (2002).

[4]M. A. Kuikka, W. Li, K. L. Kavanagh, and H.-Z. Yu, "Nanoscale electrical and structural characterization of gold/alkyl monolayer/silicon diode junctions," J. Phys. Chem. C **112**, 9081–9088 (2008).

[5]W. Hu, T. Wang, and J. Yang, "Statistical study on the Schottky barrier reduction of tunneling contacts to CVD synthesized MoS_2," J. Mater. Chem. C **3**, 4756–4761 (2015).

[6]W. Xiaozhen, F. Li, and L. Yapeng, "Effect of nano Al interlayer on the Schottky contact property between metal and $Hg_3In_2Te_6$ wafer," J. Nanosci. Nanotechnol. **15**, 7113–7116 (2015).

[7]R. Hiesgen, M. Krause, and D. Meissner, *STM Measurement of Current–Potential Curves at a Semiconductor Surface* (Elsevier, 2000), Vol. 45, pp. 3213–3223.

[8]C. Nörenberg, S. Myhra, and P. J. Dobson, "Scanning probe microscopy studies on the growth of palladium and nickel on GaN(0001)," J. Phys.: Conf. Ser. **209**(012021), 1–4 (2010).

[9]M. Hugelmann and W. Schindler, "Schottky diode characteristics of electrodeposited Au/n-Si(111) nanocontacts," Appl. Phys. Lett. **85**, 3608 (2004).

[10]M. A. Yeganeh and S. H. Rahmatollahpur, "Barrier height and ideality factor dependency on identically produced small Au/p-Si Schottky barrier diodes," J. Semicond. **31**(7), 074001 (2010).

[11]M. Jang and J. Lee, "Analysis of Schottky barrier height in small contacts using a thermionic-field emission model," ETRI **24**(6), 455–461 (2002).

[12]X.-Y. Liu and Z.-Q. Zou, "STM study of electrical transport properties of one dimensional contacts between MnSi∼1.7 nanowires and Si(111) and (110) substrates," Nanotechnology **26**, 195704 (2015).

[13]T. Lee, J. Liu, N. Po Chen, R. P. Andres, D. B. Janes, and R. Reifenberger, "Electronic properties of metallic nanoclusters on semiconductor surfaces: Implications for nanoelectronic device applications," J. Nanopart. Res. **2**, 345–362 (2000).

[14]Ch. Opoku, A. S. Dahiya, C. Oshman, C. Daumont, F. Cayrel, G. P. Vittrant, D. Alquier, and N. Camara, "Fabrication of high performance field-effect transistors and practical Schottky contacts using hydrothermal ZnO nanowires," Nanotechnology **26**, 355704 (2015).

[15]G. D. J. Smit, S. Rogge, and T. M. Klapwijk, "Scaling of nano-Schottky-diodes," Appl. Phys. Lett. **81**(20), 3852–3854 (2002).

[16]G. D. J. Smit, M. G. Flokstra, S. Rogge, and T. M. Klapwijk, Microelect. Eng. **64**, 429 (2002).

[17]M. Rezeq, K. Eledlebi, M. Ismail, B. Cui, and R. K. Dey, "Characterization of nano Schottky junctions for a new structure of nano-electronic devices," in IEEE NANO 2014, Toronto, Canada, 2014.

[18]J. Moongyu, K. Kicheon, L. Seongjae, and P. Koungwan, "Simulation of Schottky barrier tunnel transistor using simple boundary condition," Appl. Phys. Lett. **82**(16), 2718–2720 (2003).

[19]M. Wenzhe, P. Wendong, L. Pengwei, H. Jie, L. Gang, and S. Shengbo, "I-V characteristics of the metal-semiconductor junction," in International Conference on Computing, Measurement, Control and Sensor Network, 2012.

[20]R. F. Pierret, *Semiconductor Device Fundamentals* (Addison-Wesley, California, 1996), pp. 477–483 and 530–550.

[21]S. M. Sze, *Physics of Semiconductor Devices* (Wiley-Interscience Publication, New Jersey, 1981), pp. 245–260.

[22]E. H. Rhoderick and R. H. Williams, *Metal-Semiconductor Contacts* (Ckarendon Press, Oxford University, New York, 1988).